SCIENCE CHINA
Chemistry

•ARTICLES•

January 2020 Vol.63 No.1: 73–82
https://doi.org/10.1007/s11426-019-9594-y

A β-sheet-targeted theranostic agent for diagnosing and preventing aggregation of pathogenic peptides in Alzheimer's disease

Xiang Ma[1,4], Yanqing Wang[5], Jiai Hua[4], Congyu Xu[3], Tao Yang[2], Jian Yuan[1], Guiquan Chen[3*], Zijian Guo[1*] & Xiaoyong Wang[2*]

[1]*State Key Laboratory of Coordination Chemistry, School of Chemistry and Chemical Engineering, Nanjing University, Nanjing 210023, China;*
[2]*State Key Laboratory of Pharmaceutical Biotechnology, School of Life Sciences, Nanjing University, Nanjing 210023, China;*
[3]*Model Animal Research Center, Key Laboratory of Model Animal for Disease Study of Ministry of Education, Nanjing University, Nanjing 210061, China;*
[4]*Chemistry and Chemical Engineering Department, Taiyuan Institute of Technology, Taiyuan 030008, China;*
[5]*School of Chemistry and Chemical Engineering, Yancheng Teachers University, Yancheng 224002, China*

Received July 9, 2019; accepted August 22, 2019; published online October 22, 2019

Amyloid-β peptide (Aβ) aggregates, particularly Aβ oligomers, are established biomarker and toxic species in Alzheimer's disease (AD). Early detection and disaggregation of Aβ aggregates are of great importance for the treatment of AD due to the unavailability of therapy at the advanced stages of the disease. A multitalented agent, 2-{2-[(1*H*-benzoimidazol-2-yl)methoxy] phenyl}benzothiazole (BPB), is designed by merging two β-sheet targeting groups into one molecule to detect and inhibit the Aβ aggregation. BPB can quantitatively measure the β-sheet level of soluble Aβ oligomers and specifically distinguish the aggregates of Aβ40 and Aβ42 by unique luminescence spectrum. Animal tests demonstrate that BPB can efficiently penetrate the blood brain barrier and precisely stain Aβ plaques in the brain; more importantly, it can differentiate the blood of APP transgenic mice from that of normal ones. In addition to the diagnostic potential, BPB also suppresses the generation of ROS, protects the neurons from neurotoxicity, and disaggregates the Aβ aggregates in brain homogenates of APP transgenic mice induced by metal ions or self-assembly. In view of its detective ability toward Aβ oligomers and inhibition to Aβ-related neurotoxicity, BPB may be developed into a sensitive probe for screening blood samples in the early diagnosis of AD as well as an effective inhibitor for diminishing Aβ aggregates in the treatment of the disease.

Alzheimer's disease, theranostic agent, amyloid-β peptide, fluorescent probe, blood screening

Citation: Ma X, Wang Y, Hua J, Xu C, Yang T, Yuan J, Chen G, Guo Z, Wang X. A β-sheet-targeted theranostic agent for diagnosing and preventing aggregation of pathogenic peptides in Alzheimer's disease. *Sci China Chem*, 2020, 63: 73–82, https://doi.org/10.1007/s11426-019-9594-y

1 Introduction

Alzheimer's disease (AD) is an incurable neurodegenerative illness that progresses slowly into dementia and ultimately leads to death [1]. Senile plaques in the brain are the main histopathological indicator for AD [2], which is formed due to the aggregation of amyloid-β peptide (Aβ) [3]. It is believed that abnormal cerebral metal ions such as Zn^{2+} and Cu^{2+} can promote the aggregation of Aβ, and the metal-Aβ aggregates can produce reactive oxygen species (ROS) that are causative of the neuronal death [4]. Repeated failures in clinical trials of anti-AD drugs imply that it might be better to diagnose and prevent AD at the early stage rather than at the mild to moderate stages [5]. In fact, for the familial AD cohort, Aβ levels in cerebrospinal fluid (CSF) begin to dis-

*Corresponding authors (email: chenguiquan@nju.edu.cn; zguo@nju.edu.cn; boxwxy@nju.edu.cn)

order as early as 10 years before the appearance of amyloid deposits in the brain [6]. In clinical practice, senile plaques related to the progression of cognitive symptoms in AD patients are usually checked by using positron emission tomography (PET) imaging agents [7]; however, PET is unable to detect the early course of AD [8]. In addition, the expensive cost, complicated operations in producing and preserving the short-lived radioactive PET agents, and in puncturing brain to extract CSF restrict the wide application of this technique [9,10]. The early symptom of AD often involves misfolding and aggregation of Aβ monomers into oligomers [11]; and the oligomers further transmit from cell to cell or from organ to organ via the blood [12,13]. Thus, sensitive probes capable of detecting Aβ oligomers in the blood are highly needed in the preliminary screening of AD [14,15].

Aβ aggregates are both the diagnostic and therapeutic target of AD; we suppose that a combination of an Aβ-detecting agent with an Aβ-modulating agent may produce a difunctional agent that can detect and impede Aβ aggregation simultaneously [16]. Herein, we designed a potential theranostic agent, 2-{2-[(1*H*-benzoimidazol-2-yl) methoxy] phenyl}benzothiazole (BPB) (Scheme 1), which is a hybrid of 2-phenylbenzothizaole and 2-(phenoxymethyl)-1*H*-benzoimidazole, namely, analogues of Aβ-targeting thioflavin T (ThT). As expected, BPB exhibits marked ability for blood-brain barrier (BBB) penetration and excellent targeting and imaging properties for Aβ plaques *in vivo*. Aside from monitoring the soluble Aβ oligomers by fluorescence spectroscopy, it also inhibits Aβ aggregation, ROS generation and neurotoxicity. Therefore, BPB is a promising diagnostic and therapeutic agent for AD.

2 Experimental

2.1 Materials

Reagents used in this study were all of analytical grade, purchased from commercial suppliers and used as received unless otherwise stated. Human Aβ40 and Aβ42, and islet amyloid polypeptide (IAPP) were purchased from Macklin agent Ltd. (China) and verified by high performance liquid chromatography (HPLC) and electrospray ionization mass spectrometry (ESI-MS). Bovine serum albumin (BSA), human haemoglobin (Hb), myoglobin (Mb), catalase (CAT), glutathione (GSH) and oxidized glutathione (GSSG), ThT, 2′,7′-dichlorofluorescin diacetate (DCFH-DA), 3-(4,5-dimethyl-2-thiazolyl)-2,5-diphenyl-2-*H*-tetrazolium bromide (MTT), nerve growth factor 7S (NGF-7S) and tris(hydromethyl)aminomethane (Tris) were purchased from Sigma-Aldrich (USA). $Zn(OAC)_2$, $CuCl_2$, 2-phenylbenzothizaole and 2-(phenoxymethyl)-1*H*-benzoimidazole were purchased from J & K (China). Stock solutions of Aβ40, Zn^{2+} and Cu^{2+} were prepared according to the reported procedures [17], and that of BPB was prepared by dissolving the compound in dimethyl sulfoxide (DMSO) to give a final concentration of 10 mM and filtered through a filter (0.22 μm, organic system). All the solutions were prepared with Milli-Q water and filtered through a 0.22 μm filter (Millipore, USA). PC12 cells were purchased from American Type Culture Collection (ATCC). APP/PS1, APPswe and C57BL/B6 mice were purchased from the Model Animal Research Center of Nanjing University (MARC). All the animal tests were performed according to the regulations approved by MARC.

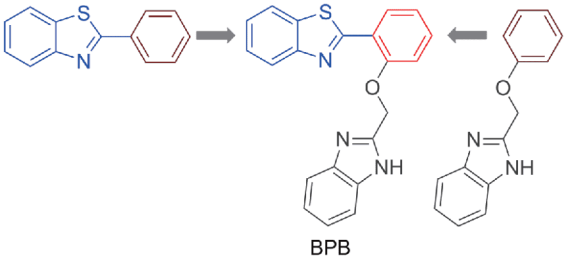

Scheme 1 Construction of BPB (color online).

2.2 Synthesis of BPB

BPB was obtained by reacting 2-(2-hydroxyphenyl)benzothiazole (0.250 g) with 2-(chloromethyl)-1-benzoimidazole (0.166 g) in the presence of K_2CO_3 (0.200 g) under acetone circumfluence (30 mL) for 8 h. The insoluble product was filtered and the filtrate was concentrated *in vacuo*. The residue was purified by silica gel column chromatography (petroleum ether/EtOAc=10:1) to obtain a colorless solid (yield: ca. 35%).

2.3 Detection of Aβ aggregates

The Aβ plaques were obtained by incubating Aβ40 (20 μM) in buffer solution (20 mM Tris-HCl/150 mM NaCl) with $Zn(OAc)_2$ (4 μL, 5 mM) at 37 °C for 24 h. BPB (10 μM) or DMSO (10 μM) was added into the system with stirring and incubated at 37 °C for 1 h. After incubation, the morphological pictures of Aβ plaques were taken by a microscope, and the corresponding fluorescence images were captured under blue light (λ_{ex}=365 nm).

2.4 Detection of Aβ oligomers

The oligomers were prepared following the reported method [18]. Aβ40 (10, 25, 40, 55, 70, 85, 100, 115, and 130 μg mL^{-1}) in the buffer solution (20 mM Tris-HCl/150 mM NaCl) was incubated at 37 °C for 24 h. After incubation, the solution was centrifuged (12,000 r min^{-1}, 4 °C, 30 min) to eliminate any fibril. BPB (1.8 μg mL^{-1}) was ad-

ded into the system with stirring, and incubated at 37 °C for 1 h. Fluorescence spectra were determined by scanning under an excitation light at 254 or 365 nm. In the interference test, the solutions of Aβ42, BSA, Hb, Mb, CAT, IAPP, GSH and GSSG (250 μg mL^{-1}) were prepared as described above and measured under the same condition.

2.5 BBB penetration and *in vivo* imaging

BPB in saline solution (DMSO 5%) was administered to the 10-month-old APP/PS1 transgenic mice and B6-mice through the tail vein injection at a dose of 30 mg kg^{-1}. The brain tissues and blood were collected at 4 h after injection. Histological staining of the brain slices was obtained by immunohistochemistry assay according to the literature [19]. The morphological pictures of senile plaques in the slices were captured by a microscope; and the corresponding fluorescence images were captured under an ultraviolet (λ_{ex}= 254 nm) and blue light (λ_{ex}=365 nm) respectively.

The blood was drawn from the eye socket of mice and centrifugalized at 4 °C and 7,000 r min^{-1} for 15 min. The blood plasma was separated and diluted in buffer solution (20 mM Tris-HCl/150 mM NaCl, 1: 4). Fluorescence spectra were observed at an excitation light at 365 nm.

2.6 Inhibition of Aβ aggregation

2.6.1 Turbidity

Aβ40 (20 μM) in buffer solution (20 mM Tris-HCl/150 mM NaCl) was incubated with or without $Zn(OAc)_2$ or $CuCl_2$ (4 μL, 5 mM) at 37 °C for 5 min. BPB (4 μL, 10 mM) or DMSO (4 μL) was added into the system with stirring and incubated at 37 °C for 24 h. Each sample was transferred to a well of a flat-bottomed 96-well plate. Turbidity of the solution was measured using the absorbance at 405 nm. Data were expressed as mean±standard deviations of at least three independent experiments.

2.6.2 Morphological analysis

Sample solutions were prepared in the same way as described in the turbidity test. An aliquot of solution (10 μL) was spotted on the 300-mesh carbon-coated copper grids for 2 min at room temperature and the excess sample was removed. Each grid was stained with uranyl acetate (10 μL, 1%, *w*/*v*) for 1 min and washed with Milli-Q water (10 μL), and then was examined on a JEOL JEM-2100 LaB6 (HR) transmission electron microscope (Japan).

2.6.3 Analysis of brain homogenates

Brain extracts of 7-month-old APPswe transgenic mice were prepared according to the reported procedure [20]. Briefly, the extracted brain tissue pieces were homogenized in NP40 buffer (Tris-HCl, 50 mM; NaCl, 150 mM; NP40, 1%; Na-deoxycholate, 0.25%; 1 mM of EDTA, Na_3VO_4, NaF; 1 μg mL^{-1} of aprotinin, leupeptin, pepstatin; and 1 mM of fresh PMSF). The homogenate solutions were centrifuged at 12,000 r min^{-1} and 4 °C for 10 min, and the resulting supernatant was collected. BPB (0.2, 0.4, 0.6, 0.8, 1.0 and 1.2 μM) and DMSO (final concentration 1%) were added respectively to the supernatant (100 μL). After incubation at 37 °C for 24 h, the samples were dissolved in loading buffer containing β-mercaptoethanol (5%) and boiled at 95 °C for 10 min. Each sample was separated by sodium dodecylsulphate polyacrylamide gel electrophoresis (SDS-PAGE) and transferred onto polyvinylidene difluoride (PVDF) membranes. The membranes were blocked for 0.5 h at room temperature with fat-free milk (5%) and then incubated at 4 °C for 12 h with monoclonal anti-Aβ antibody 6E10 (1:1,000, Covance Inc.). The bolts were then incubated with the HRP-conjugated goat anti-mouse antibody (1:1,000) for 1 h at room temperature. Bands were visualized using ChemiScope 3400 Mini (CLiNX Science Instruments Co., Ltd.). Glyceraldehyde-phosphate dehydrogenase (GAPDH) at the same concentration as in the mouse homogenate was used as an internal reference to ensure the equal protein loading. The membranes were then developed using an enhanced chemiluminescence detection kit, stripped and rechecked with GAPDH antibody (1:5,000; Meridian Life Sciences, Canada).

2.7 Reduction of neurotoxicity

2.7.1 Inhibition of ROS generation

DCFH stock solution (1 mM) was prepared with a buffer (20 mM Tris-HCl/150 mM NaCl, pH 7.4) according to the reported procedures [20]. Horseradish peroxidase (HRP) stock solution (4 μM) was prepared with the same buffer. Sample solutions containing Aβ40 (20 μM) and $CuCl_2$ (20 μM) were incubated with or without BPB (40 μM) at 37 °C. Ascorbate (10 μM) was added to each sample and incubated at 37 °C for 10 min. The sample (200 μL) was transferred to the wells of a flat-bottomed 96-well black plate. HRP (0.04 μM) and DCFH (100 μM) were added to each solution and incubated in the dark at 37 °C. Fluorescence intensity (λ_{ex}=485 nm, λ_{ex}=650 nm) was measured by a Varioskan Flash microplate reader (Thermo Scientific, USA) every 10 min from 0 to 2,400 min.

2.7.2 Inhibition of neurotoxicity

The PC12 cells used for the neurotoxicity and synaptic dysfunction analysis were prepared as described previously [21]. The inhibition effect of BPB on the neurotoxicity was evaluated using PC12 cells by the MTT assay. PC12 cells were incubated with Aβ40 (20 μM) alone or with Zn^{2+}- or Cu^{2+}(20 μM)-induced Aβ40 complexes in the absence or presence of BPB (40 μM) for 24 h.

2.7.3 Inhibition of synaptic dysfunction

PC12 cells were prepared as described above. After incubation for 24 h, the morphological pictures of the cells were captured by a microscope.

2.8 Interaction mode

2.8.1 Molecular docking

The molecular simulations were performed by the blind docking calculations using the Autodock software [22]. The crystallographic data of Aβ40 and Aβ42 fibrils were obtained from the Protein Data Bank (http://www.rcsb.org/pdb/explore/explore.do?StructureId=2lmo). Gaussian 09 was used to optimize the three-dimensional structure of BPB at DFT B3LYP/LanL2DZ base level. Autodock 4.2.3 program was used to perform the blind docking calculations of Aβ fibrils with BPB. A grid box of 80 Å×80 Å×80 Å with spacing of 0.357 Å was used to enclose compound and Aβ fibrils. The Lamarckian Genetic Algorithm method was used as the searching algorithm. PyMOL software was used to analyze the predicated binding mode [Delano, W.L. The PyMol Molecular Graphic System, DeLano Scientific, San Carlos, CA, USA, 2004, http://pymol.sourceforge.net.].

2.8.2 Isothermal titration calorimetry (ITC)

ITC was performed on a NANO ITC system (TA Instruments Inc., USA) according to the literature method [3]. Titrations were performed in buffer (20 mM Tris-HCl/150 mM NaCl, pH 7.4). Injections of BPB (40 μL, 600 μM, 2% DMSO) were completed by a computer controlled microinjector at an interval of 150 s for Aβ42 (20 μM) and 190 s for Aβ40 (20 μM) under stirring at 25 °C. The experiment data were analyzed with NanoAnalyze software and fitted to an independent model concurrently with a blank constant model to adjust for the heat of dilution.

2.8.3 Metal chelating ability

Aβ40 (20 μM) was dissolved in the buffer solution (20 mM Tris-HCl/150 mM NaCl, pH 7.4) and incubated with Zn^{2+} or Cu^{2+} (4 μL, 5 mM) in the presence of BPB (4 μL, 10 mM) at 37 °C for 24 h. The solution was loaded on the chromatographic column and the saline ions were washed off by Milli-Q water. The products were collected using an acid solution composed of 75% acetonitrile, 20% Milli-Q water and 5% acetic acid. The peptide solution was examined on an LCQ Fleet electrospray mass spectrometer.

2.8.4 Conformational transformation

Sample solutions were prepared in the same way as described in the turbidity test. The CD spectra of the solutions were recorded on a JASCO J-810 automatic recording spectropolarimeter (Tokyo, Japan) in the range of 195–270 nm. The data acquired in the absence of protein were subtracted from the spectrum.

3 Results and discussion

3.1 Design and synthesis of BPB

Lipinski ever suggested that in the design of anti-AD agents, several parameters should be taken into consideration, such as molecular weight (MW) and calculated partition coefficient (Clog*P*) [23,24]. To obtain an optimal molecule that conforms with the Lipinski's rule, molecular merging might be a wise option because it would save unnecessary atoms and reach desired properties more concisely. In the design of BPB, two ThT derivatives, viz. 2-phenylbenzothiazole and 2-(phenoxymethyl)-1*H*-benzoimidazole, were used to form the hybrid molecule; both units could act as Aβ-targeting groups as well as Aβ-imaging and metal chelating groups [25,26]. We suppose that their combination could enhance the binding affinity and imaging ability for Aβ; furthermore, the coordination atoms could snatch metal ions from Aβ aggregates and thereby inhibiting the Aβ aggregation. Since planar structures are likely to insert the β-sheet of Aβ aggregate, BPB may interact directly with Aβ and hence alter its fluorescence emission and prohibit the Aβ self-misfolding [27]. The synthetic route to BPB is shown in Scheme S1 (Supporting Information online). BPB was formed by reacting 2-(2-hydroxyphenyl)benzothiazole with 2-(chloromethyl)-1-benzoimidazole in the presence of K_2CO_3 under acetone circumfluence, and was characterized by NMR and ESI-MS (Figures S1 and S2, Supporting Information online). As shown in Table 1, the molecular parameters of BPB coincide well with the Lipinski's rule and the calculated logBB is 0.19, suggesting that BPB is likely to penetrate the BBB [23,24].

3.2 Detection of Aβ aggregates

Since BPB contains two analogues of ThT, it should possess the targeting and sensing ability for the β-sheet of Aβ. Aβ monomers could assemble into aggregates such as oligomers, protofibrils and plaques, among which the soluble β-sheet-rich oligomers are the most toxic species [28]. Therefore, the detection of the soluble β-sheet-rich Aβ aggregates is important for diagnosing and monitoring the state of AD. The fluorescence response of BPB to Aβ40 in solution is shown in Figure 1. Two strong peaks were observed at ca. 395 and 500 nm after BPB was incubated with Aβ40, indicating that Aβ40 can significantly enhance the fluorescence of BPB. The intensity of the peaks increased rapidly and correlated linearly with the concentration of Aβ40 from 5 to 60 μg mL^{-1}. When the concentration of Aβ40 surpassed 60 μg mL^{-1}, a new linear relationship appeared (inset of Figure 1). The change of the linear relationship may arise

Table 1 MW, Clog*P*, hydrogen-bond acceptor (HBA), hydrogen-bond donor (HBD), polar surface area (PSA), and logBB values of BPB and reference data according to the Lipinski's rule

	MW	Clog*P* [a)]	HBA	HBD	PSA [a)]	logBB [b)]
BPB	357	4.82	3	1	45.98	0.19
Ref.	≤450	≤5	≤10	≤5	≤90	

a) Clog*P* and PSA are predicted by the Discovery Studio 2.5 Software (Accelrys); b) logBB=–0.0148×PSA+0.152×Clog*P*+0.139.

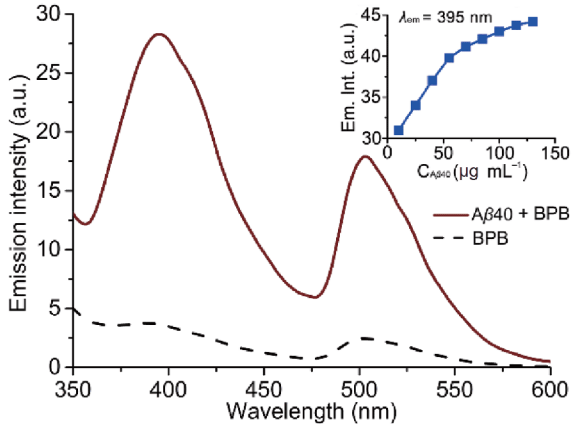

Figure 1 Fluorescence emission of BPB (1.8 μg mL^{-1}) in the absence and presence of Aβ40 (5 μg mL^{-1}) (λ_{ex}=254 nm), and the correlation of emission intensity of BPB with the concentration of Aβ40 at 395 nm (inset) (color online).

from the different Aβ-binding abilities of the 2-phenylbenzothiazole and benzoimidazole moieties in BPB, with the former being greater than the latter and easy to be saturated in the combination with Aβ aggregates. The composition of the Aβ40 solution was identified by PAGE. The molecular weights of the aggregates are in the range of 10–15 kDa (Figure S3), indicating that Aβ40 existed in oligomers, such as dimers, trimers or tetramers. These results suggest that BPB is highly sensitive to the soluble Aβ40 oligomers in solution.

To test the selectivity of BPB, the fluorescence emission spectra of BPB in the presence of Aβ42, BSA, Hb, Mb, CAT, IAPP, GSH and GSSG were determined and compared with that in the presence of Aβ40 under the same condition. Short peptides or proteins rich in α-helix, such as GSH, GSSG, Hb and Mb, barely increase the fluorescence of BPB; BSA and CAT can enhance the fluorescence at about 395 nm with no characteristic peak (Figure S4). However, as shown in Figure 2, peptides rich in β-sheet can enhance the fluorescence of BPB, for example, the peak at 395 nm is significantly increased and blue-shifted to 345 nm by IAPP, but the intensity is weaker than that induced by Aβ40. Interestingly, two peaks are observed at 510 and 535 nm when BPB is incubated with Aβ42, while only one peak is observed in this region for Aβ40. The different responses of BPB to Aβ42 and Aβ40 may be attributed to the distinction of secondary structure and amino acid sequence [29]. Aβ42 has two more hydrophobic amino acid residues, that is, Ile and Ala, at positions 41 and 42 [5]. Aβ tends to form hydrophobic β-sheet, with hydrophobic groups being folded outward; the additional Ile and Ala would make Aβ42 to form β-sheet more readily than Aβ40 [25]. The difference in the secondary structure of Aβ42 and Aβ40 results in not only the different responses of BPB to Aβ42 and Aβ40 (*vide infra*), but also the higher toxicity of Aβ42 [11].

To the best of our knowledge, BPB seems to be a rare sensor that can differentiate Aβ40 from Aβ42. Since immoderate increase of Aβ42 is a crucial inducement of early Aβ aggregation [30], the ratio of Aβ42 to Aβ40 is considered as an important biomarker for initial AD [31]. Hence, BPB could be used to evaluate the risk factors of AD and diagnose the process of AD in the clinic. Formerly reported fluorescence probes usually show an enhancement or recession of the fluorescence [27], reflecting the bioactive metal ions in the solution [32]. The different responses of BPB to various peptides suggest that BPB not only detects the total level of β-sheets but also distinguishes Aβ40 and Aβ42 by characteristic fluorescence spectra.

When BPB was excited with light at 365 nm, it could mark the Aβ40 plaques precisely by emitting green fluorescence. As shown in Figure 3, the Aβ plaques and the fibrous materials surrounding the plaques are visible and distinguishable easily (Figure 3(a, c)). By contrast, no emission is captured without BPB (Figure 3(b, d)). The results indicate that BPB can specifically stain Aβ deposits and produce significant fluorescence.

3.3 BBB penetration and *in vivo* imaging

BBB is the main obstruction for developing anti-AD agents because most drug candidates cannot cross it [33]. To test the BBB-penetrating ability of BPB, we injected it intravenously into the 10-month-old amyloid precursor protein/presenilin protein 1 (APP/PS1) transgenic mice and determined its existence by staining the senile plaques confirmed by the Aβ antibody. As shown in Figure 4, a lot of senile plaques exist in the brain of mouse and no fluorescence is observed at excitation wavelength of 254 or 365 nm without BPB (Figure 4(a, c, e)); by contrast, most of the senile plaques are lightened 4 h after the intravenous injection of BPB, indicating that BPB can penetrate the BBB and stain the senile plaques specifically *in vivo* (Figure 4(b, d, f)).

Soluble β-sheet-rich Aβ oligomers are the main cause of synaptic dysfunction and memory loss in AD [34]. It has been demonstrated that Aβ oligomers can migrate with blood to some organs such as eyes [13]. Thus, the level of Aβ oligomers in blood is a potential biomarker for the diagnosis of AD [13–15]. Since BPB can detect soluble Aβ oligomers quantitatively in the buffer, we further studied its sensing

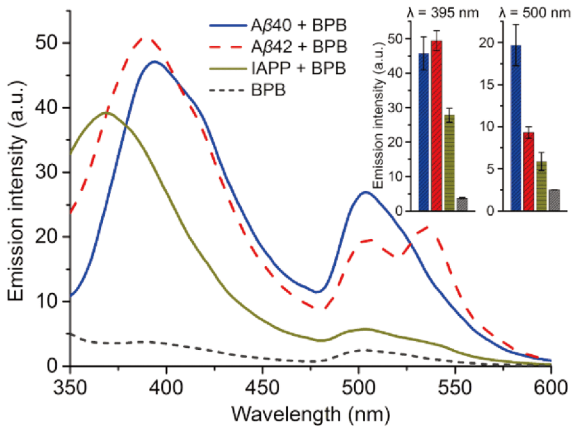

Figure 2 Fluorescence spectra of BPB (1.8 μg mL^{-1}) in the absence or presence of different proteins (250 μg mL^{-1}, λ_{ex}=254 nm) in the buffer (5 mM Tris-HCl, 50 mM NaCl, pH 7.4) and the emission intensity at 395 and 500 nm (inset) (color online).

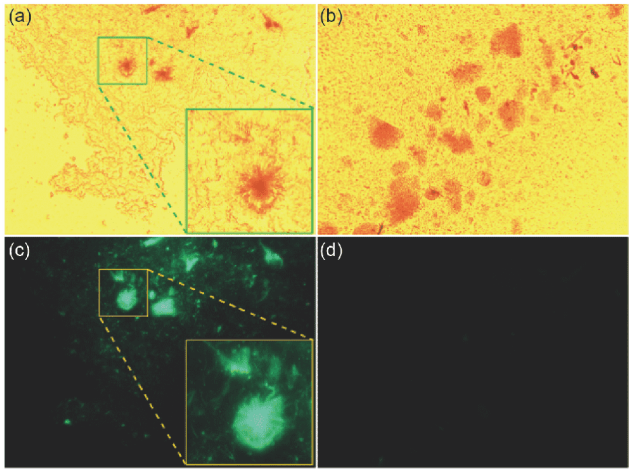

Figure 3 Photomicrographs (a, b) and corresponding fluorescence images (c, d) (λ_{ex}=365 nm) of Aβ40 fibrils and plaques stained with (a, c) or without (b, d) BPB (color online).

ability in a blood sample. As shown in Figure 5, a weak fluorescence peak is observed at about 500 nm at 4 h after BPB was injected intravenously into normal B6-type mice. However, a strong fluorescence peak is observed at about 500 nm after BPB was injected intravenously into APP/PS1 mice, with the intensity being 10-fold stronger than that of the normal B6-type control. The injection of saline into both B6- and APP/PS1 mice did not induce fluorescence in this region. These results indicate that BPB can detect Aβ oligomers in blood and differentiate the blood of APP/PS1 mice from that of normal ones. As compared with the mice injected with physiological saline, no untoward effect was observed on the mice after the injection of BPB at a dosage of 30 mg kg^{-1} every 5 d for two weeks. The mice only showed a mild lethargy with an injection of 80 mg kg^{-1}, thus indicating that BPB is highly biocompatible.

To date, most of Aβ fluorescence probes can only detect

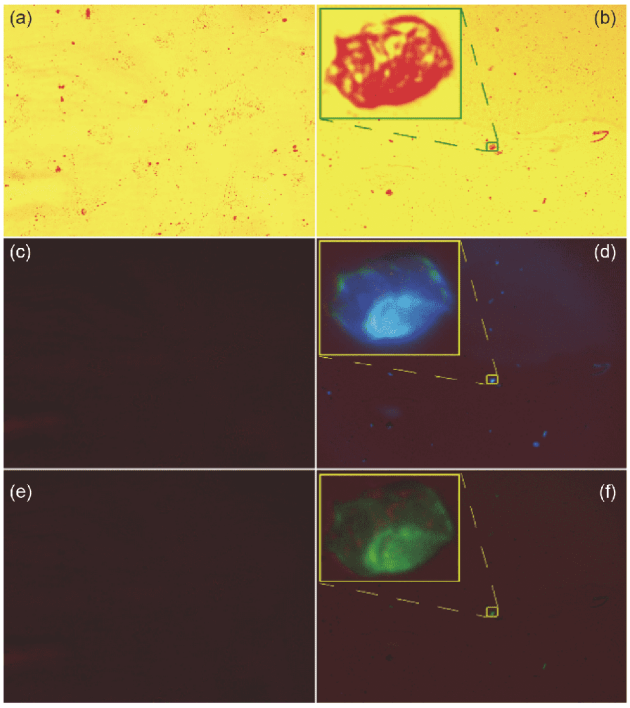

Figure 4 Histological staining images of the brain slices from 10-month-old APP/PS1 transgenic mice (20×, inset 400×). (a) Mice (light field); (b) mice+PBP (light field); (c) mice (λ_{ex}=254 nm); (d) mice+PBP (λ_{ex}=254 nm); (e) mice (λ_{ex}=365 nm); (f) mice+PBP (λ_{ex}=365 nm) (color online).

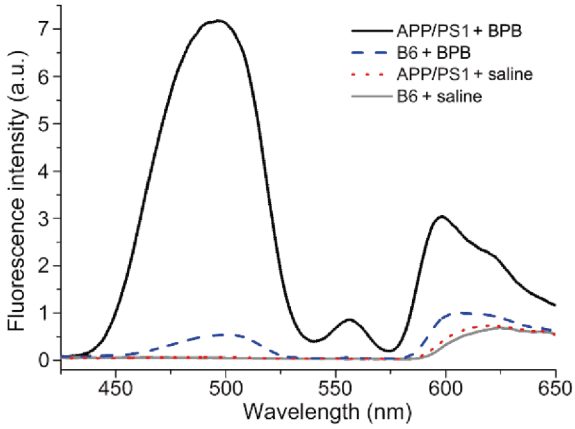

Figure 5 Fluorescence spectra (λ_{ex}=365 nm) of blood plasma from APP/PS1 transgenic or normal B6-type mice at 4 h after intravenous injection with BPB (30 mg kg^{-1}) or saline (color online).

the senile plaques *in vitro*, which is only applicable to pathological slice researches [25,35]. Uniquely, BPB can distinguish the blood of AD mice from the normal samples. Since blood samples are readily available, BPB may serve as an economical and facile testing tool to diagnose or monitor the development of AD at the early stage.

3.4 Inhibition of Aβ aggregation

In addition to the Aβ-sensing ability, we also examined the inhibitory effect of BPB on the Zn^{2+}- or Cu^{2+}-induced Aβ

aggregation by determining the turbidity or UV-Vis absorbance of the Aβ40 solutions at 405 nm (A_{405}), which reflects the level of all types of Aβ aggregates [17]. The turbidity increased considerably after incubation with Zn^{2+} or Cu^{2+} as compared with that of the metal-free Aβ40 solution (Figure S5), which is consistent with our previous observations [20]. In the presence of BPB, the turbidity markedly decreased, particularly when induced by Zn^{2+}, which indicates that BPB can inhibit Zn^{2+}- or Cu^{2+}-induced Aβ40 aggregation. The morphology of Aβ40 and Zn^{2+}- or Cu^{2+}-induced Aβ40 aggregates in the absence or presence of BPB was analyzed by transmission electron microscopy (TEM). Large amounts of amyloid deposits or fibrils were observed when Aβ40 was incubated with Zn^{2+} (Figure 6(a)) or Cu^{2+} (Figure 6(b)), which are consistent with previous reports [20,36]. Aβ40 produced some fibrils in solution (Figure 6(c)). The difference between Zn^{2+}- and Cu^{2+}-induced aggregates may be attributed to the different aggregation mechanisms [26]. In the presence of BPB, Aβ40 only formed small amounts of amorphous deposits with Zn^{2+} or with Cu^{2+} (Figure 6(d, e)), indicating that BPB can inhibit the Aβ aggregation induced by Zn^{2+} or Cu^{2+} ions. Only several fragments were observed after Aβ40 was incubated with BPB (Figure 6(f)), implying that BPB also interferes with the self-aggregation of Aβ.

To further verify the inhibitory effect of BPB on the Aβ aggregation in real bio-samples, the brain homogenates of 7-month-old APPswe transgenic mice were analyzed by Western blotting after treatment with BPB. As shown in Figure 7, a dark band is observed at ca. 130 kDa in the control group, and some ambiguous bands are observed in the molecular weight (MW) region of 55–130 kDa. The results indicate that Aβ aggregates in different maturity stages coexist in the brain homogenates of the APPswe mice, with species of 130 kDa being the dominant component, which is consistent with the previous report [37]. After treatment with BPB (Lanes 1–6), however, the bands in the high MW region (130–55 kDa) became pale while that at ca. 12 kDa became dark with the increase of BPB. These changes indicate that BPB can disassemble the Aβ aggregates with high MW and convert them into low MW species, which is in accord with the above morphological analysis.

3.5 Reduction of neurotoxicity

ROS are the major species accounting for the neurotoxicity in AD [38–40]. The effect of BPB on the Cu^{2+}-Aβ mediated ROS generation was thus investigated by a dichlorofluorecin (DCF) assay. DCF is a fluorescent marker derived from the reaction of non-fluorescent 2′,7′-dichlorofluorecin (DCFH) with ROS in the presence of horseradish peroxidase (HRP), which can indicate the total output of ROS from the Cu^{2+}-Aβ complex [20]. As shown in Figure 8, the fluorescence intensity of DCF incubated with Cu^{2+}-Aβ is higher than that

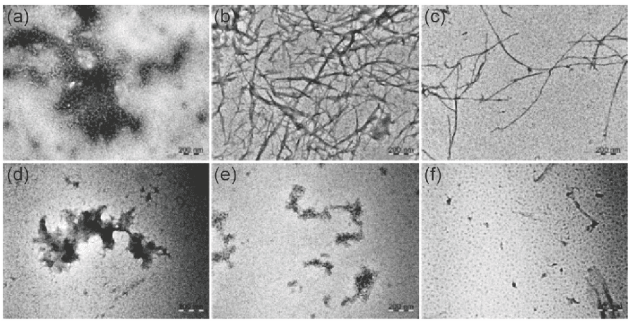

Figure 6 TEM images of Zn^{2+}- or Cu^{2+}-treated Aβ40 samples (20 μM) in the absence or presence of BPB after incubation at 37 °C and pH 7.4 for 24 h, respectively ([Aβ40]:[metal ion]:[BPB]=1:1:2), with Aβ40 as the control. (a) Aβ40+Zn^{2+}; (b) Aβ40+Cu^{2+}; (c) Aβ40; (d) Aβ40+Zn^{2+}+BPB; (e) Aβ40+Cu^{2+}+BPB; (f) Aβ40+BPB.

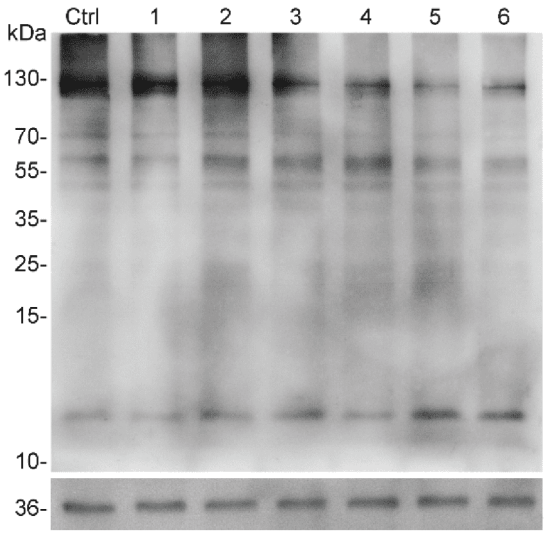

Figure 7 Immunoblots of brain homogenates from APPswe transgenic mice in SDS-PAGE after treatment with BPB (Lanes 1–6: 0.2, 0.4, 0.6, 0.8, 1.0 and 1.2 μM, respectively) analyzed by Western blotting with the anti-Aβ anti-body 6E10.

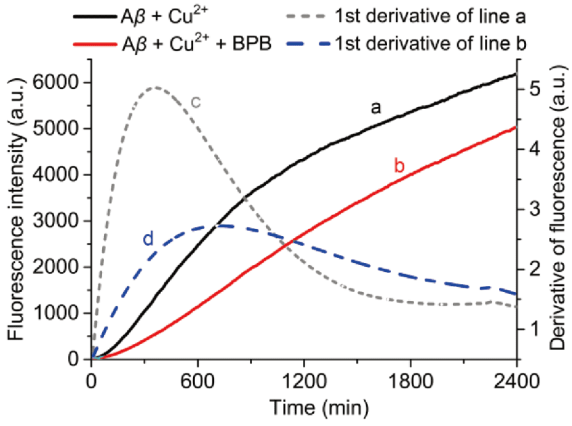

Figure 8 Fluorescence intensity of DCF (λ_{ex}=485 nm, λ_{em}=525 nm) induced by Cu^{2+}+Aβ40 (a) or Cu^{2+}+Aβ40+BPB (b), and the 1st derivative of line a (c) and line b (d) at 0–2400 min (color online).

incubated with Cu^{2+}-Aβ plus BPB, indicating that the production of ROS without BPB is more than that with BPB. The instantaneous inhibition rate is also described by the 1st derivative of fluorescence intensity. From 0 to 600 min, the ROS production rate of Cu^{2+}-Aβ without BPB is ca. 2.5 times higher than that with BPB. These results reveal that BPB can efficiently inhibit the ROS generation from the Cu^{2+}-Aβ complex.

The protective effect of BPB on the synapsis was investigated by analyzing the morphological changes of neuronal pheochromocytoma PC12 cells after incubation with Zn^{2+}- or Cu^{2+}-induced Aβ40 aggregates with BPB. As shown in Figure 9, PC12 cells take polygonal shapes with neurites (control) [41]. After treatment with Zn^{2+}- or Cu^{2+}-Aβ40 complexes or Aβ40 for 24 h, the cell body and the neurites shrank, and the dendritic networks were disrupted (Figure 9 (a, d, g)). However, in the presence of BPB, the cells incubated with metal-Aβ40 complexes or Aβ40 almost maintain the same shape as the untreated cells (Figure 9(b, e, h)). Zn^{2+}/Cu^{2+} and BPB barely influence the shape of cells in the absence of Aβ40 (Figure 9(c, f)), indicating that BPB is low toxic to the cells.

Recent studies showed that Aβ can induce synaptic toxicity, leading to the dysfunction of neuron cells without killing them [42,43]. Here we demonstrate that BPB can protect the neurons from synaptic toxicity induced by Zn^{2+}- or Cu^{2+}-Aβ40 aggregates, or self-assembled aggregates. The cellular viability of PC12 cells determined by the MTT assay [44,45] in the presence of Aβ40, Zn^{2+}/Cu^{2+}, and BPB also showed that BPB can reduce the neurotoxicity induced by metal-Aβ40 or Aβ40 alone (see Figure S6).

3.6 Interaction mode

To understand the interaction between BPB and Aβ40/42, we adopted the crystallographic data of Aβ40 and Aβ42 and optimized the geometry of BPB to perform the blind docking calculations using the Autodock software [22]. As shown in Figure 10(a, c, e), there are nine amino acid residues, Val-18, Ser-8, Phe-19, Phe-4, His-6, Glu-22, Gln-15, Asp-7 and Arg-5, taking part in the interactions of Aβ40 with BPB. Among them, Val-18, Phe-4 and Phe-19 are hydrophobic, and the rest are hydrophilic, implying that hydrophobic and van der Waals forces as well as hydrogen bonding are involved in the interaction. Three hydrogen bonds exist between BPB and Gln-15 (2.8635 Å), Asp-7 (2.9712 Å) or Arg-5 (2.6375 Å). In addition, π-π stacking exists between the benzothiazole aromatic ring of BPB and Phe-19 residue. Figure 10(b, d, f) shows that there are five amino acid residues, Val-12, Phe-19, Lys-16, Glu-11 and Gln-15, taking part in the interactions of Aβ42 with BPB. Among them, Val-12 and Phe-19 are hydrophobic, and two hydrogen bonds exist between BPB and Glu-11 (3.2042 Å) or Val-12 (3.0611 Å). Moreover, π-π

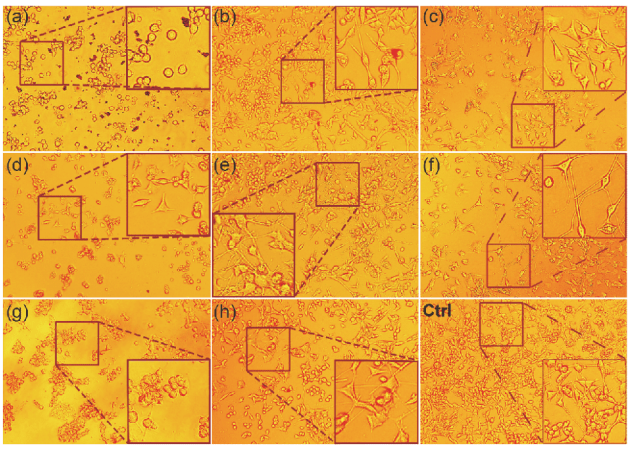

Figure 9 Photomicrographs of PC12 cells after incubation with Zn^{2+}- or Cu^{2+}-induced Aβ40 aggregates with or without BPB ([Aβ40]=[Cu^{2+}]=[Zn^{2+}]=20 μM, [BPB]=40 μM). (a) Aβ40+Zn^{2+}; (b) Aβ40+Zn^{2+}+BPB; (c) Zn^{2+}+BPB; (d) Aβ40+Cu^{2+}; (e) Aβ40+Cu^{2+}+BPB; (f) Cu^{2+}+BPB; (g) Aβ40; (h) Aβ40+BPB (color online).

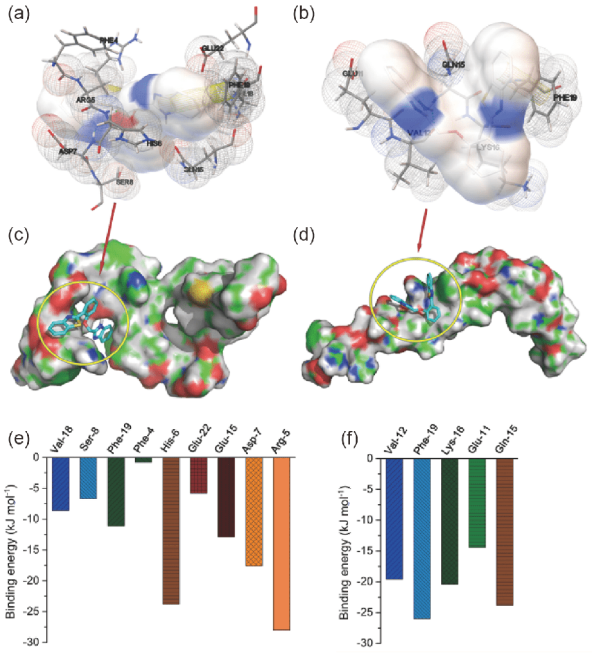

Figure 10 Detailed surroundings of BPB-Aβ40 and BPB-Aβ42 complexes represented in ball-and-stick (a, b) and space-filling (c, d) modes, respectively, and the lowest binding free energy corresponding to related amino acid residues in BPB-Aβ40 (e) and BPB-Aβ42 (f) complexes (color online).

stacking also exists between benzimidazole aromatic ring of BPB and Phe-19 residue. The two additional hydrophobic groups in Aβ42 changed the folding mode of polypeptide, thereby affecting the π-π stacking modes and intensity between BPB and Phe-19 residue, which may result in the difference in the fluorescence spectra of BPB corresponding to Aβ40 and Aβ42 respectively. The results also suggest that the interference of Aβ self-aggregation by BPB may arise from the weak interactions between BPB and amino acid

residues in Aβ40 or Aβ42.

The binding between BPB and Aβ42 or Aβ40 was further studied by ITC according to the literature method [3]. The binding was exothermic and fit for a 1:1 binding mode, and the binding constant (K) of BPB to Aβ42 and Aβ40 was calculated to be 1.86×10^4 and 1.36×10^4, respectively, on the ITC data (Figure S7). The binding free energy was −24.36 and −23.58 kJ mol^{-1} for Aβ42 and Aβ40, respectively. The results indicate that there are weak interactions between BPB and Aβ42 or Aβ40, which is consistent with the above molecular simulations. The slight difference between the binding free energy of Aβ42- and Aβ40-BPB (0.78 kJ mol^{-1}) may result from the distinct insertion mode of BPB to Aβ42 and Aβ40.

The interactions of BPB with Zn^{2+}- or Cu^{2+}-induced Aβ40 were investigated by ESI-MS. The peaks of metal-Aβ40 complexes after incubation with BPB are shown in Figure S8 and the attributions are summarized in Tables S1 and S2 (Supporting Information online). Cu^{2+}- and Zn^{2+}-Aβ40 complexes produced similar peaks after incubation with BPB, indicating that BPB can coordinate with Zn^{2+} or Cu^{2+} and form similar adducts (Figure S9). Further study clarified that it is N rather than S atom of 2-(2-hydroxyphenyl)benzothiazole that coordinated with Zn^{2+}/Cu^{2+} (Figure S10), which is in agreement with the literature [46]. These results indicate that BPB dissociates the metal-induced Aβ plaques by despoiling Zn^{2+} or Cu^{2+} from the Aβ aggregates.

Finally, the effect of BPB on the conformation of Aβ40 in the presence of metal ions was investigated by using circular dichroism (CD) spectrometry. As shown in Figure 11, a negative band is observed at 215 nm after Aβ40 was incubated with Cu^{2+} for 24 h, which indicates that Aβ40 is in the β-sheet conformation [47]. The CD spectrum became more negative after Aβ40 was incubated with Zn^{2+}, indicating that the conformational transformation is greatly aggravated by Zn^{2+}. However, in the presence of BPB, the spectra of Aβ40 showed an obvious recession in negative bands, indicating that BPB can convert the β-sheet conformation of Aβ aggregates with or without metal ions. It is acknowledged that the formation of toxic Aβ oligomers or fibrils often involves a conformational conversion of Aβ from unordered forms or α-helix into β-sheet, which is a crucial process in the pathogenesis of AD [48]. Most of the reported monofunctional chelators only prevent the formation of metal-Aβ complex but do not interact with Aβ *per se*, and hence have no effects on Aβ self-aggregation [17,26,35]. BPB acts not only as a chelator but also as an interfering agent on the formation of β-sheets. Since the two constituent parts of BPB are planar structures, they may insert into the misfolded Aβ by π-π stacking, and thereby prevent the misfolded Aβ from becoming a template for further aggregation [27,49], leading to the changes in fluorescence.

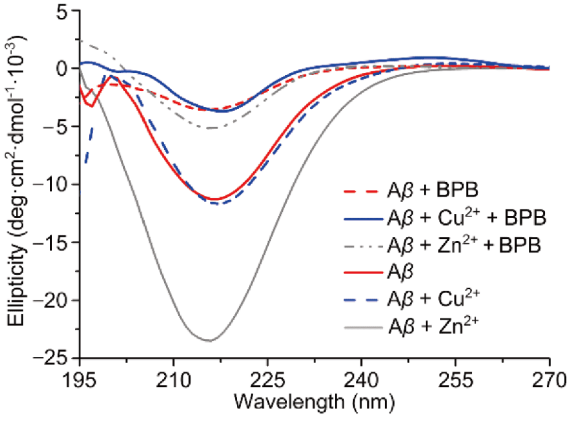

Figure 11 CD spectra of Aβ40 (20 μM) with or without Cu^{2+} or Zn^{2+} (20 μM) and BPB (40 μM) after incubation at 37 °C for 24 h (color online).

4 Conclusions

The treatment of Alzheimer's disease (AD) could benefit from the identification of biomarkers at the prodromal stage. Soluble Aβ oligomers play a key role in the AD onset. Thus, the detection and inhibition of Aβ oligomers are of great significance in the early diagnosis and prevention of AD. In this study, we described an Aβ-targeted multifunctional fluorescent probe (BPB) with both diagnostic and therapeutic potentials for AD. BPB can detect the soluble Aβ oligomers in the blood plasma by fluorescence spectroscopy, which may be used to examine the biomarker of AD at early stage or monitor the therapeutic effect during the treatment. Moreover, BPB can penetrate the blood brain barrier and stain the senile plaques efficiently in mouse model, which provides an effective tool for exploring the neuropathology of AD associated with Aβ aggregation. Along with these features, BPB can prevent the self-assembly or metal-induced aggregation of Aβ and suppress the production of ROS induced by Cu-Aβ species, thus reducing the neurotoxicity of Aβ aggregates and protecting the neurons from synaptic loss.

Recently, some compounds with excellent fluorescent properties have been developed for the diagnosis of AD [50]. In comparison with these probes, BPB has some unique properties. Firstly, it can differentiate the blood of APP transgenic mice from that of normal ones by fluorescence spectroscopy; secondly, it may be used to expediently screen potential AD patients at early stages instead of using complicated methods such as examining cerebrospinal fluid and brain tissue slice; and finally, it possesses remarkable inhibitory ability against Aβ aggregation. Therefore, BPB is a potential diagnostic and therapeutic agent for AD.

Acknowledgements This work was supported by the National Natural Science Foundation of China (21877059, 31570809, 21731004), the

National Basic Research Program of China (2015CB856300), the Natural Science Foundation of Jiangsu Province (BK20150054), and the Research Foundation of the Chinese State Key Laboratory of Coordination Chemistry (SKLCC1912).

Conflict of interest The authors declare that they have no conflict of interest.

Supporting information The supporting information is available online at http://chem.scichina.com and http://link.springer.com/journal/11426. The supporting materials are published as submitted, without typesetting or editing. The responsibility for scientific accuracy and content remains entirely with the authors.

1 Kepp KP. *Chem Rev*, 2012, 112: 5193–5239
2 Vinters HV. *Annu Rev Pathol Mech Dis*, 2015, 10: 291–319
3 Gao N, Sun H, Dong K, Ren J, Duan T, Xu C, Qu X. *Nat Commun*, 2014, 5: 3422–3431
4 Faller P, Hureau C, La Penna G. *Acc Chem Res*, 2014, 47: 2252–2259
5 Selkoe DJ. *Science*, 2012, 337: 1488–1492
6 Bateman RJ, Xiong C, Benzinger TLS, Fagan AM, Goate A, Fox NC, Marcus DS, Cairns NJ, Xie X, Blazey TM, Holtzman DM, Santacruz A, Buckles V, Oliver A, Moulder K, Aisen PS, Ghetti B, Klunk WE, McDade E, Martins RN, Masters CL, Mayeux R, Ringman JM, Rossor MN, Schofield PR, Sperling RA, Salloway S, Morris JC. *N Engl J Med*, 2012, 367: 795–804
7 Tentolouris-Piperas V, Ryan NS, Thomas DL, Kinnunen KM. *Brain Res*, 2017, 1655: 23–32
8 Selkoe DJ. *Nat Med*, 2011, 17: 1060–1065
9 Zhu L, Ploessl K, Kung HF. *Chem Soc Rev*, 2014, 43: 6683–6691
10 Johnson KA, Fox NC, Sperling RA, Klunk WE. *Cold Spring Harb Perspect Med*, 2012, 2: a006213
11 Selkoe DJ, Hardy J. *EMBO Mol Med*, 2016, 8: 595–608
12 Guo JL, Lee VMY. *Nat Med*, 2014, 20: 130–138
13 Ratnayaka JA, Serpell LC, Lotery AJ. *Eye*, 2015, 29: 1013–1026
14 Clark LF, Kodadek T. *Alzheimer's Res Ther*, 2013, 5: 18–25
15 Wood H. *Nat Rev Neurol*, 2016, 12: 678
16 Telpoukhovskaia MA, Orvig C. *Chem Soc Rev*, 2013, 42: 1836–1846
17 Chen T, Wang X, He Y, Zhang C, Wu Z, Liao K, Wang J, Guo Z. *Inorg Chem*, 2009, 48: 5801–5809
18 Santos MJ, Quintanilla RA, Toro A, Grandy R, Dinamarca MC, Godoy JA, Inestrosa NC. *J Biol Chem*, 2005, 280: 41057–41068
19 Cheng S, Hou J, Zhang C, Xu C, Wang L, Zou X, Yu H, Shi Y, Yin Z, Chen G. *Sci Rep*, 2015, 5: 10535–10549
20 Wang X, Wang X, Zhang C, Jiao Y, Guo Z. *Chem Sci*, 2012, 3: 1304–1312
21 Yang T, Wang X, Zhang C, Ma X, Wang K, Wang Y, Luo J, Yang L, Yao C, Wang X. *Chem Commun*, 2016, 52: 2245–2248
22 Trott O, Olson AJ. *J Comput Chem*, 2010, 31: 455–461
23 van de Waterbeemd H, Gifford E. *Nat Rev Drug Discov*, 2003, 2: 192–204
24 Clark DE, Pickett SD. *Drug Discov Today*, 2000, 5: 49–58
25 Rodriguez-Rodriguez C, Sanchez de Groot N, Rimola A, Alvarez-Larena A, Lloveras V, Vidal-Gancedo J, Ventura S, Vendrell J, Sodupe M, Gonzalez-Duarte P. *J Am Chem Soc*, 2009, 131: 1436–1451
26 Savelieff MG, DeToma AS, Derrick JS, Lim MH. *Acc Chem Res*, 2014, 47: 2475–2482
27 Zhang X, Tian Y, Li Z, Tian X, Sun H, Liu H, Moore A, Ran C. *J Am Chem Soc*, 2013, 135: 16397–16409
28 Gao N, Qu XG. *Sci Sin Chim*, 2018, 48: 941–955
29 Economou NJ, Giammona MJ, Do TD, Zheng X, Teplow DB, Buratto SK, Bowers MT. *J Am Chem Soc*, 2016, 138: 1772–1775
30 Bibl M, Esselmann H, Mollenhauer B, Weniger G, Welge V, Liess M, Lewczuk P, Otto M, Schulz JB, Trenkwalder C, Kornhuber J, Wiltfang J. *J Neurochem*, 2007, 103: 467–474
31 Urraca JL, Aureliano CSA, Schillinger E, Esselmann H, Wiltfang J, Sellergren B. *J Am Chem Soc*, 2011, 133: 9220–9223
32 Wang J, Wang Y, Hu X, Zhu C, Ma Q, Liang L, Li Z, Yuan Q. *Anal Chem*, 2019, 91: 823–829
33 Chen Y, Liu L. *Adv Drug Deliver Rev*, 2012, 64: 640–665
34 Haass C, Selkoe DJ. *Nat Rev Mol Cell Biol*, 2007, 8: 101–112
35 Hickey JL, Lim SC, Hayne DJ, Paterson BM, White JM, Villemagne VL, Roselt P, Binns D, Cullinane C, Jeffery CM, Price RI, Barnham KJ, Donnelly PS. *J Am Chem Soc*, 2013, 135: 16120–16132
36 Kochi A, Eckroat TJ, Green KD, Mayhoub AS, Lim MH, Garneau-Tsodikova S. *Chem Sci*, 2013, 4: 4137–4145
37 Ma X, Hua J, Wang K, Zhang H, Zhang C, He Y, Guo Z, Wang X. *Inorg Chem*, 2018, 57: 13533–13543
38 Barnham KJ, Bush AI. *Chem Soc Rev*, 2014, 43: 6727–6749
39 Atrián-Blasco E, Del Barrio M, Faller P, Hureau C. *Anal Chem*, 2018, 90: 5909–5915
40 Yang L, Sun J, Xie W, Liu Y, Liu J. *J Mater Chem B*, 2017, 5: 5954–5967
41 Chen Q, Yang L, Zheng C, Zheng W, Zhang J, Zhou Y, Liu J. *Nanoscale*, 2014, 6: 6886–6897
42 Hong S, Beja-Glasser VF, Nfonoyim BM, Frouin A, Li S, Ramakrishnan S, Merry KM, Shi Q, Rosenthal A, Barres BA, Lemere CA, Selkoe DJ, Stevens B. *Science*, 2016, 352: 712–716
43 Tanzi RE. *Nat Neurosci*, 2005, 8: 977–979
44 Fu AKY, Hung KW, Yuen MYF, Zhou X, Mak DSY, Chan ICW, Cheung TH, Zhang B, Fu WY, Liew FY, Ip NY. *Proc Natl Acad Sci USA*, 2016, 113: E2705–E2713
45 Tan MS, Tan L, Jiang T, Zhu XC, Wang HF, Jia CD, Yu JT. *Cell Death Dis*, 2014, 5: e1382
46 Yu G, Yin S, Liu Y, Shuai Z, Zhu D. *J Am Chem Soc*, 2003, 125: 14816–14824
47 Li M, Howson SE, Dong K, Gao N, Ren J, Scott P, Qu X. *J Am Chem Soc*, 2014, 136: 11655–11663
48 Ono K, Condron MM, Teplow DB. *Proc Natl Acad Sci USA*, 2009, 106: 14745–14750
49 Zhao DS, Chen YX, Liu Q, Zhao YF, Li YM. *Sci Sin Chim*, 2012, 42: 226–228
50 (a) Lv G, Sun A, Wei P, Zhang N, Lan H, Yi T. *Chem Commun*, 2016, 52: 8865–8868; (b) Chan HN, Xu D, Ho SL, Wong MS, Li HW. *Chem Sci*, 2017, 8: 4012–4018; (c) Yin Z, Wang S, Shen B, Deng C, Tu Q, Jin Y, Shen L, Jiao B, Xiang J. *Anal Chem*, 2019, 91: 3539–3545